

Low Temperature Thermodynamic Properties of the Heavy Fermion Compound YbAgGe Close to the Field-Induced Quantum Critical Point

Y. Tokiwa[¶], A. Pikul^{¶‡}, P. Gegenwart[¶], F. Steglich[¶], S.L. Bud'ko*, and P.C. Canfield*

[¶]*Max-Planck Institute for Chemical Physics of Solids, D-01187 Dresden, Germany*

[‡]*Institute of Low Temperature and Structure Research,*

Polish Academy of Sciences, 50-950 Wrocław, Poland

**Ames Laboratory US DOE and Department of Physics and Astronomy,*

Iowa State University, Ames, IA 50011, USA

(Dated: May 11, 2018)

Abstract

We present temperature and field dependent heat capacity and magnetization data taken at temperatures down to 50 mK and in an applied magnetic field up to 11.5 Tesla for YbAgGe, a heavy-fermion compound with a field induced quantum critical point. These data clearly indicate that the same electronic degrees of freedom are responsible for the features seen in both specific heat and magnetization data. In addition, they further refine the different boundaries suggested for the $H - T$ phase diagram of YbAgGe through previous, magneto-transport measurements, and allow for further understanding of different phases on the $H - T$ phase diagram, in particular, clearly disconnecting the field-induced quantum critical point in YbAgGe from any sort of saturation of the Yb moment in higher applied magnetic field.

PACS numbers: 75.20.Hr, 75.30.Mb

I. INTRODUCTION

YbAgGe was recently recognized to be one of the few stoichiometric Yb-based heavy fermion compounds that demonstrates field-induced non-Fermi-liquid (NFL) behavior as evidenced by thermodynamic and transport measurements in an applied magnetic field [1]. In zero applied field YbAgGe has two (small magnetic moment) magnetic ordering transitions, at ≈ 1 K and ≈ 0.65 K [1, 2, 3], with the latter one being first order. The magnetic ordering temperatures are well separated from the Kondo temperature ($T_K \sim 25$ K) that is itself well below the estimated first excited CEF level ($T_{CEF} \sim 60 - 100$ K) [4, 5]. The anisotropic $H - T$ phase diagrams for YbAgGe were constructed based on heat capacity measurements down to 400 mK and magnetotransport measurements down to temperatures of ≈ 50 mK [1, 3, 6, 7, 8], and the nature of some of the magnetic phases has been probed by recent neutron scattering measurements [9, 10]. Whereas the general outline of these phase diagrams is similar to the generic $H - T$ phase diagram for the materials with a quantum critical point (QCP) (see *e.g.* Ref. 11), (i) they have an additional line, defined by a clear anomaly in the Hall effect measurements [6, 8], that apparently originates at the QCP (a similar line was also suggested for YbRh₂Si₂ [12]); (ii) the apparent non-Fermi-liquid (NFL) region does not collapse to a point in the $T \rightarrow 0$ limit, but spans a magnetic field range of several Tesla [1, 7, 8].

With this complex phase diagram in mind and lacking detailed neutron scattering data covering a wide $H - T$ domain, field- and temperature-dependent magnetization measurements gain an additional importance in the case of the field-induced QCP, allowing for the clear identification of the saturated paramagnetic state (if reached) and often giving supplementary information on the intermediate, magnetic-field-induced, phases. Whereas in the previous publications magnetotransport data have been collected for $T \geq 50$ mK and $H \leq 18$ T [1, 3, 6, 7, 8] and $C_p(T, H)$ results so far exist in the $T \geq 400$ mK and $H \leq 14$ T domain [1, 3], systematic magnetization data have only been collected for $T \geq 1.8$ K. To address this critical gap in the data set, the core of this work is a set of $M(H, T)$ data covering the vicinity of the QCP. In addition, in order to compare these magnetization data with another, key, thermodynamic quantity, additional heat capacity data were taken over the same $H - T$ range.

II. EXPERIMENTAL

YbAgGe single crystals in the form of clean, hexagonal-cross-section rods of several mm length and up to 1 mm^2 cross section were grown from high temperature ternary solutions rich in Ag and Ge (see [2] for details of the samples' growth). Their structure and full site-occupancy, without any detectable site-disorder, were confirmed by single crystal X-ray diffraction [13]. DC-magnetization of a single crystalline sample of YbAgGe was measured down to $\approx 0.05 \text{ K}$ and in high fields up to 11.5 T using a high-resolution capacitive Faraday magnetometer [14]. The specific heat measurements were carried out down to $\approx 0.05 \text{ K}$ in magnetic fields up to 11 T using the compensated quasi-adiabatic heat pulse method [15]. For both measurements the magnetic field was applied perpendicular to the crystallographic c -axis, *i.e.* along the basal, ab plane.

III. RESULTS AND DISCUSSION

A representative set of temperature-dependent M/H data is shown in Figs. 1,2. The small, low temperature upturn in the low-field data (Fig. 1) is possibly caused by a very small amount of paramagnetic impurities (consistent with the shape of $M(H)$ in the low-field region - not shown here). This upturn disappears by $H = 1 \text{ T}$. The lower, first order, magnetic transition ([1, 2, 3]) is clearly seen in the low field susceptibility data (Fig. 1). It shifts to lower temperatures with an increase of applied field, and the width of the hysteresis increases. It is worth mentioning that for $H = 0.1 \text{ T}$ a relatively sharp change of slope is observed slightly below 1 K (insert to Fig. 1). This feature marks the higher temperature magnetic transition.

The lower temperature transition is not detectable in the temperature-dependent susceptibility measurements taken in applied fields of 2 T and higher (Fig. 2). The functional behavior of the susceptibility clearly changes when applied field increases from 2 T to 11 T. Up to 4 T a magnetic transition can be followed by monitoring the maximum in $d(M/H)/dT$; For $H \geq 6 \text{ T}$ the magnetic susceptibility increases with decrease of temperature with the trend to saturation below $\sim 1 \text{ K}$. The 5 T susceptibility behaves similarly to the higher field ones with an additional feature near 0.5 K.

All in all the temperature-dependent susceptibility data is consistent with the $H - T$

phase diagram for $H||ab$ suggested in Refs. 1, 3, 6, 7, 8 (shown with these data added in Fig. 8 below) with qualitative changes in the functional behavior when the first order transition is suppressed ($H \sim 2$ T) and at the critical field, H_{QCP} , when the second order phase transition is suppressed.

A representative $M(H)$ data set is presented in Fig. 3(a). A well-defined kink at ~ 4.5 T is evident in the raw data for $T = 0.05$ K curve. This anomaly broadens with increasing temperature. The magnetization at 11.5 T, for the whole range of temperatures, shows only the initial signs of possibly approaching a saturation. This set of data is consistent with the published $T = 0.45$ K [3] as well as the $T = 2$ K [1] $M(H)$ curves.

The low field, first order phase transition can also be clearly detected in the $M(H)$ data. This is shown in Figure 4 where an enlargement of a field-up / field-down sweep is shown. This transition is even more clearly seen in the dM/dH plot shown on the same panel, the right hand axes.

On a broader scale, the derivatives of the magnetization isotherms, dM/dH (Fig. 3(b)), allow for a closer look at the features in magnetization and their evolution with temperature. As discussed above, the narrow peaks in dM/dH at and below 2 T (for $T \leq 0.5$ K) indicate the phase line associated with the lower, first order, magnetic transition. In addition, an asymmetric peak below 5 T is clearly seen in the 0.05 K, 0.25 K and 0.39 K curves (marked by arrows); this feature evolves into a less pronounced, high slope feature at 0.5 K (marked with an arrow) with a broad maximum (*) appearing at ~ 5 T. This broad maximum persists up to at least 3 K. Additionally, a smaller maximum (∇) can be observed for the dM/dH data taken at 0.25 K and 0.39 K near 3 T. In higher fields, *e.g.* $H \approx 7$ T for the 0.05 K curve, a broad shoulder in dM/dH is also observed. This shoulder is only marginally detectable for $T = 0.5$ K and lack of high field data for the intermediate temperatures does not allow to follow its evolution with temperature.

The low temperature part of the temperature-dependent heat capacity in constant applied magnetic field is shown in Fig. 5. All the data below ~ 200 mK show an upturn that corresponds to nuclear contributions to the specific heat. The data above ~ 400 mK are consistent with the previously reported heat capacity data [1]. For $H = 4$ T, the onset of magnetic order can still be clearly seen in the heat capacity data (marked with an arrow in Fig. 5).

From the $C_p(T)$ data taken in different fields we can assemble $C(H)/T$ data and plot

them together with the differential susceptibility, $\chi = dM/dH$. Fig. 6 illustrates that, at least over some $H - T$ range, these two quantities are proportional to each other, with a constant proportionality factor. This implies that the C/T data as well as the dM/dH data emerge from the same electronic degrees of freedom. It should be noted that the magnetic transition is at least as clearly seen in the C/T vs. H as in the dM/dH curves (Fig. 6). In order to follow this proportionality to lower temperatures the nuclear contributions to the specific heat (Schottky, hyperfine) were subtracted. The nuclear specific heat $C_{nuc} = \alpha/T^2$ was determined by fitting CT^2 data at low temperatures, below 0.1 K, with $\alpha + \gamma T^3$. The resulting data are shown in Figure 7. As can be seen, below 300 mK the $\Delta C_p/T$ data are essentially temperature-independent (Fig. 7(a), inset). It should be noted that within the framework of this background subtraction, this temperature independence of $\Delta C_p/T$ is in contrast to the clear linear in temperature resistivity [7] in parts of this $H - T$ region. This allows for the estimation of $\Delta C_p/T$ for $T = 0.05$ K. These data are compared to dM/dH at the same temperature. As can be seen in Fig. 7(b), the proportionality between C_p/T and dM/dH appears to extend down to our lowest measured temperatures. On the other hand, it breaks down for temperatures of 1 K and higher (Fig. 6). This is the same temperature range in which the temperature-dependent resistivity measured in different applied magnetic fields allows for a single-power-law fit [7]. It should be noted that an accurate assessment of the Sommerfeld - Wilson ratio, $R = 4\chi\pi^2k_B^2/3\gamma\mu_{eff}^2$, from the data in Fig. 6 is hampered by the anisotropy of the magnetic susceptibility in YbAgGe and ambiguity of the μ_{eff} value in the $H - T$ domain of the aforementioned data. If forced to do it, the evaluation using the high temperature $\mu_{eff} = 4.54\mu_B$ (an overestimate for the low temperature μ_{eff}) will result in the (underestimated) Sommerfeld - Wilson ratio value $R \approx 1$.

Further examination of the Fig. 6 reveals the shoulder at $\sim 6 - 7$ T in the C/T data (as well as in the base temperature, 50 mK, dM/dH data in Fig. 3(b)). A similar anomaly in dM/dH and $\gamma(H)$, observed in YbRh₂Si₂ [16], was associated with a suppression of the heavy fermion state; this was coincident with the saturation of the magnetization and it was argued that this helped confirm the field-induced localization of f -electrons. Such an association is not appropriate for YbAgGe where the saturation of the magnetization data is not yet reached by 11 T (Fig. 3(a)). The shoulder in Fig. 6 may be a sign of some field-induced Fermi surface changes. Additionally, it is worth mentioning that the Sommerfeld - Wilson ratio is usually constant when the sample is in the Fermi-liquid regime. Earlier

thermodynamic and transport measurements in YbAgGe [1, 7, 8] suggest that for $H\parallel ab$ the Fermi-liquid regime in this material sets up at $H = 9 - 10$ T, significantly above the field of 4.5 - 5 T at and above which the constant Sommerfeld - Wilson ratio is observed (Fig. 6). Additional theoretical and experimental efforts are required for further understanding of the ground state of YbAgGe in the intermediate field range, but it appears that the features in dM/dH as well as C/T that occur in the non-Fermi liquid and Fermi-liquid regimes originate from the same electronic degrees of freedom.

Fig. 8 shows the $H - T$ phase diagram for YbAgGe ($H\parallel ab$) [7, 8] overlaid by the aforementioned features. All magnetic phase lines are seen in the magnetization measurements. The hysteresis of the lower magnetic transition increases with decrease of temperature and magnetic field. The Hall line that originates at the field-induced QCP [6, 8] appears to have a corresponding, broad feature in dM/dH , that very poorly manifests itself in the raw $M(H)$ data. The Hall line at higher fields coincides with the shoulders in both the dM/dH and the C/T data. At this point these phase lines consistently manifest themselves in magnetization, specific heat, magnetoresistance and Hall effect measurements.

IV. SUMMARY

Temperature- and field-dependent magnetization measurements performed on YbAgGe single crystals with the magnetic field in the basal plane confirm the magnetic phase lines suggested by the electrical transport and specific heat measurements in applied field. The Hall line that originates at the field-induced QCP [6, 8] has a correspondent feature in dM/dH data as well, and this feature extends to temperatures above the zero applied field magnetic ordering temperature. For all studied temperature range ($50 \text{ mK} \leq T \leq 2 \text{ K}$) the magnetization does not saturate below 11 T, suggesting that the Yb moment is not saturated in the $H - T$ domain of these measurements, and the Yb magnetic moment saturation is not associated with the field induced QCP in this material. The observed proportionality of the differential susceptibility and the linear-in-temperature coefficient of specific heat clearly indicates that the same electronic degrees of freedom are responsible for the features seen in both sets of data not only in the Fermi liquid regime, but also in the lower field, non-Fermi liquid region.

Acknowledgments

Ames Laboratory is operated for the U.S. Department of Energy by Iowa State University under Contract No. W-7405-Eng.-82. Work at Ames Laboratory was supported by the Director for Energy Research, Office of Basic Energy Sciences. A. Pikul is indebted to the Alexander von Humboldt Foundation for a research fellowship.

- [1] S. L. Bud'ko, E. Morosan, and P. C. Canfield, *Phys. Rev. B* **69**, 014415 (2004).
- [2] E. Morosan, S. L. Bud'ko, P. C. Canfield, M. S. Torikachvili, and A. H. Lacerda, *J. Magn. Magn. Mat.* **277**, 298 (2004).
- [3] K. Umeo, K. Yamane, Y. Muro, K. Katoh, Y. Niide, A. Ochiai, T. Morie, T. Sakakibara, and T. Takabatake, *J. Phys. Soc. Jpn.* **73**, 537 (2004).
- [4] K. Katoh, Y. Mano, K. Nakano, G. Terui, Y. Niide, and A. Ochiai, *J. Magn. Magn. Mat.* **268**, 212 (2004).
- [5] T. Matsumura, H. Ishida, T. J. Sato, K. Katoh, Y. Niide, and A. Ochiai, *J. Phys. Soc. Jpn.* **73**, 2967 (2004).
- [6] S. L. Bud'ko, E. Morosan, and P. C. Canfield, *Phys. Rev. B* **71**, 054408 (2005).
- [7] P. G. Niklowitz, G. Knebel, J. Flouquet, S. L. Bud'ko, and P. C. Canfield, cond-mat/0507211.
- [8] S. L. Bud'ko, V. Zapf, E. Morosan, and P. C. Canfield, cond-mat/0507338.
- [9] B. Fåk, D. F. McMorrow, P. G. Niklowitz, S. Raymond, E. Ressouche, J. Flouquet, P. C. Canfield, S. L. Bud'ko, Y. Janssen, and M. J. Gutmann, *J. Phys.: Condens. Matter* **17**, 301 (2005).
- [10] B. Fåk, P. G. Niklowitz, D. F. McMorrow, C. Rüegg, S. Raymond, J. Flouquet, P. C. Canfield, S. L. Bud'ko, and Y. Janssen, in: *Proceedings of SCES'05, Vienna*.
- [11] M. A. Continentino, G. Japiassu, and A. Troper, *Phys. Rev. B* **39**, 9734 (1989).
- [12] S. Paschen, T. Lühmann, S. Wirth, P. Gegenwart, O. Trovarelli, C. Geibel, F. Steglich, P. Coleman, and Q. Si, *Nature* **432**, 881 (2004).
- [13] Y. Mozharivskij, private communication.
- [14] T. Sakakibara, H. Mitamura, T. Tayama, and H. Amitsuka, *Jpn. J. Appl. Phys.* **33**, 5067 (1994).

- [15] H. Wilhelm, T. Lühmann, T. Rus, and F. Steglich, *Rev. Sci. Instr.* **75**, 2700 (2004).
- [16] Y. Tokiwa, P. Gegenwart, T. Radu, J. Ferstl, G. Sparn, C. Geibel, and F. Steglich, *Phys. Rev. Lett.* **94**, 226402 (2005).

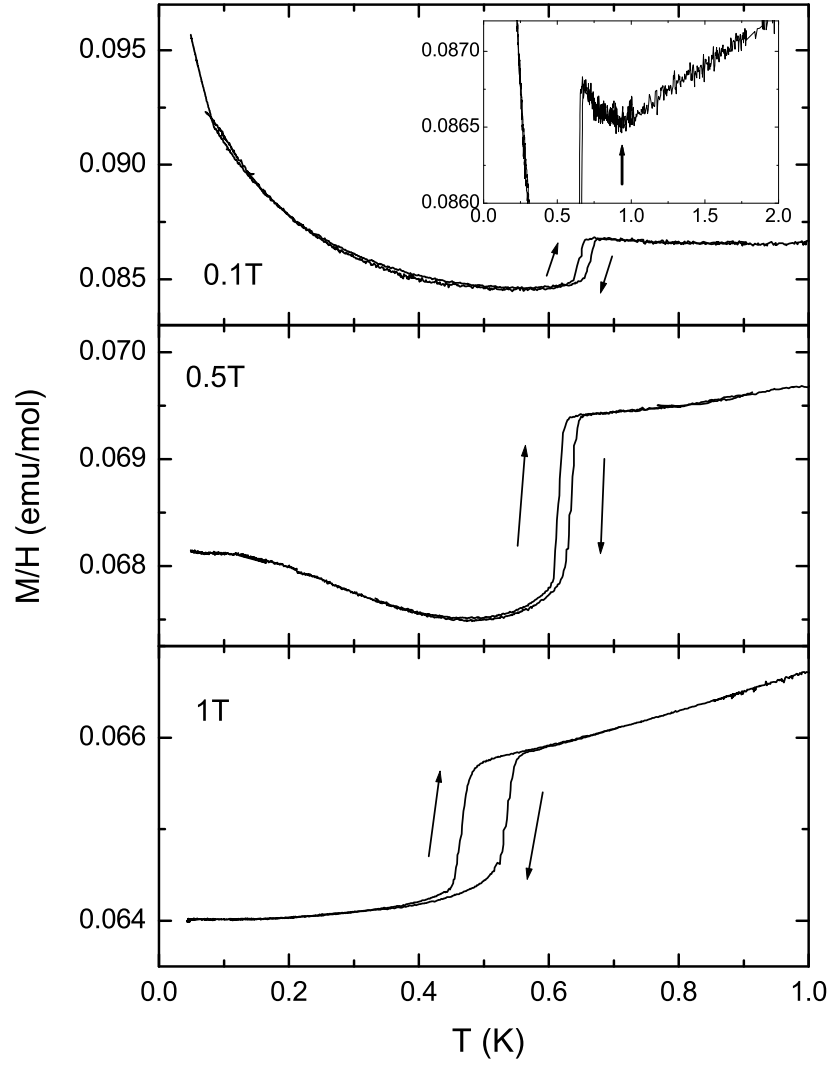


FIG. 1: Representative plots of the low-field temperature dependent susceptibility of YbAgGe ($H \parallel ab$, $H \leq 1$ T) below 1 K. Arrows mark data taken on increase/decrease of temperature. Inset shows break of slope near 1 K in $H = 0.1$ T data.

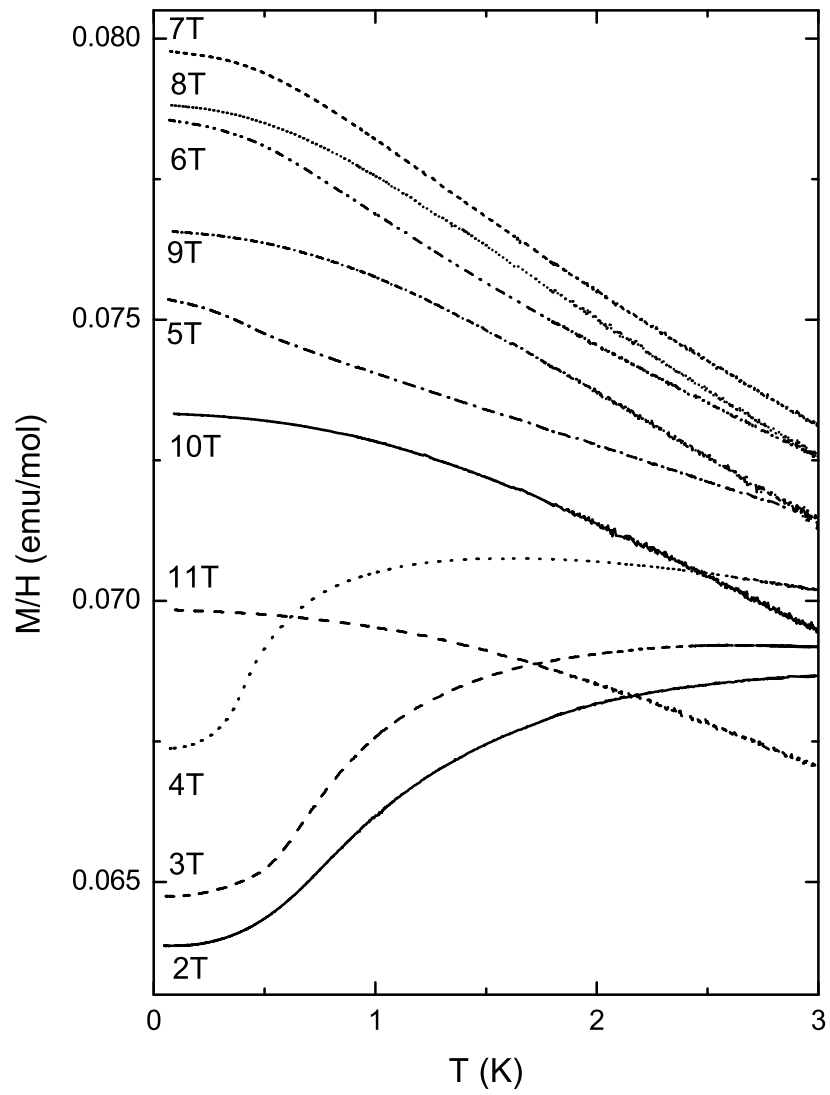
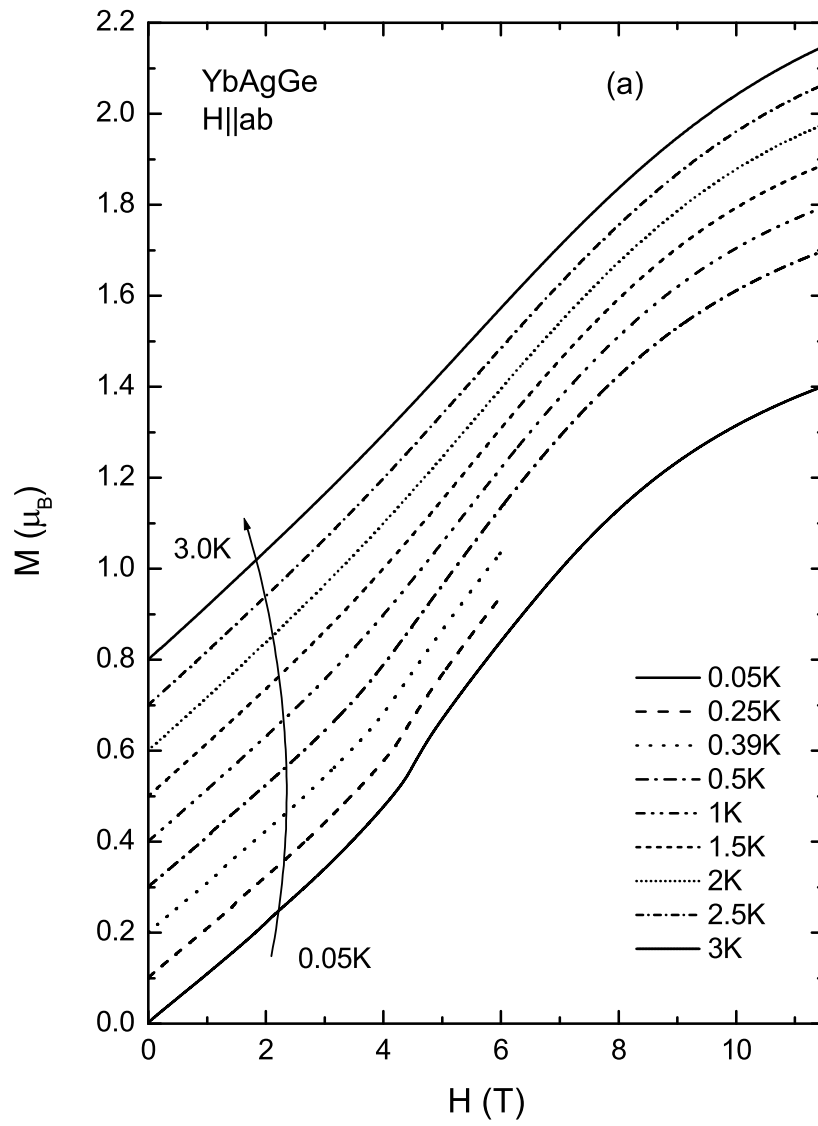


FIG. 2: Temperature dependent susceptibility of YbAgGe in magnetic fields between 2T and 11 T ($H \parallel ab$) below 3 K. Data taken on temperature increase.



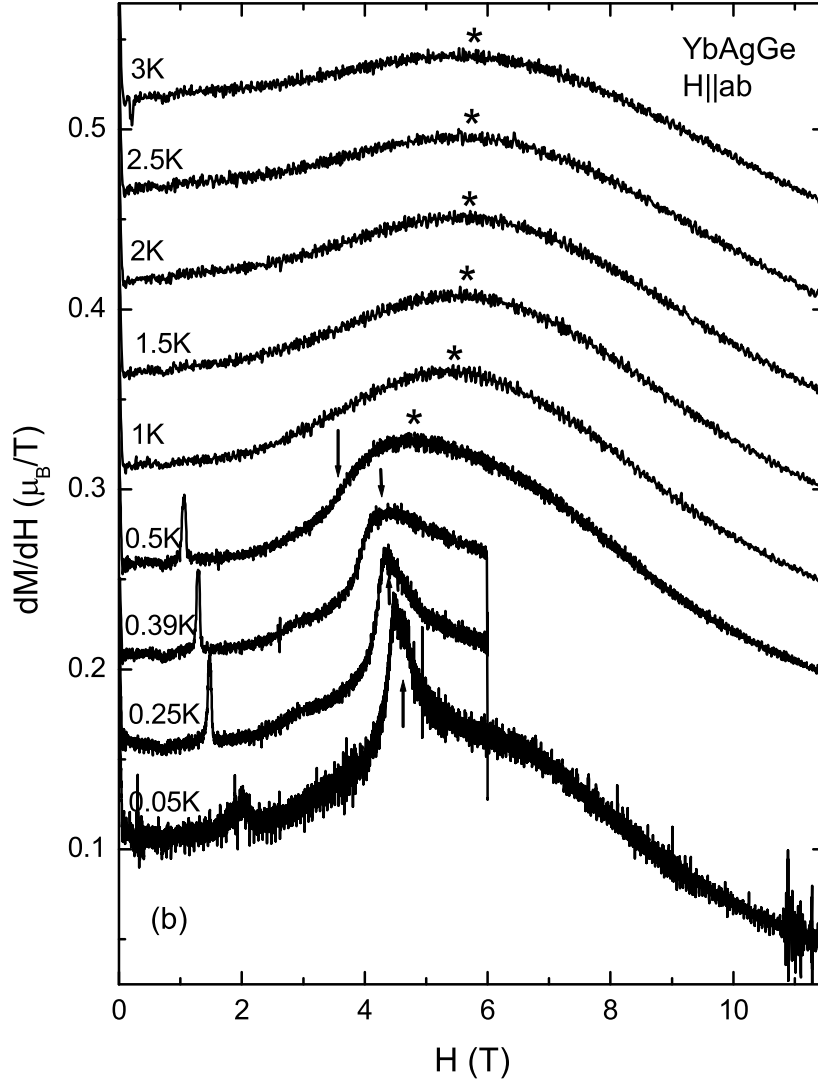


FIG. 3: (a) Representative plots of low-temperature field-dependent magnetization, $M(H)$, of YbAgGe ($H||ab$). Curves are shifted along the y -axis by multiplicative factors of $0.1 \mu_B$ for clarity; (b) dM/dH derivatives for the representative $M(H)$ taken on increase of the magnetic field - curves for $T \geq 0.25$ K have an offset by a multiplicative of $0.05 \mu_B/T$ for clarity (see text for the discussion of different features).

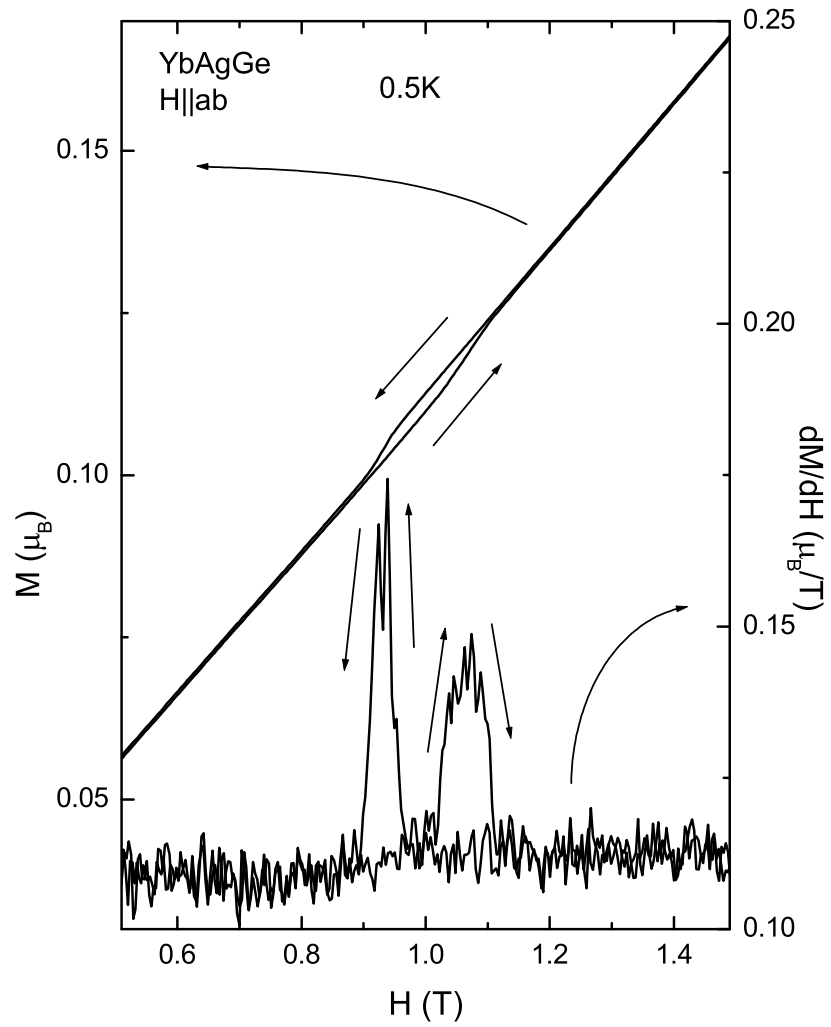


FIG. 4: Example of hysteretic low field/low temperature transition as seen in raw $M(H)$ data and in the derivative dM/dH .

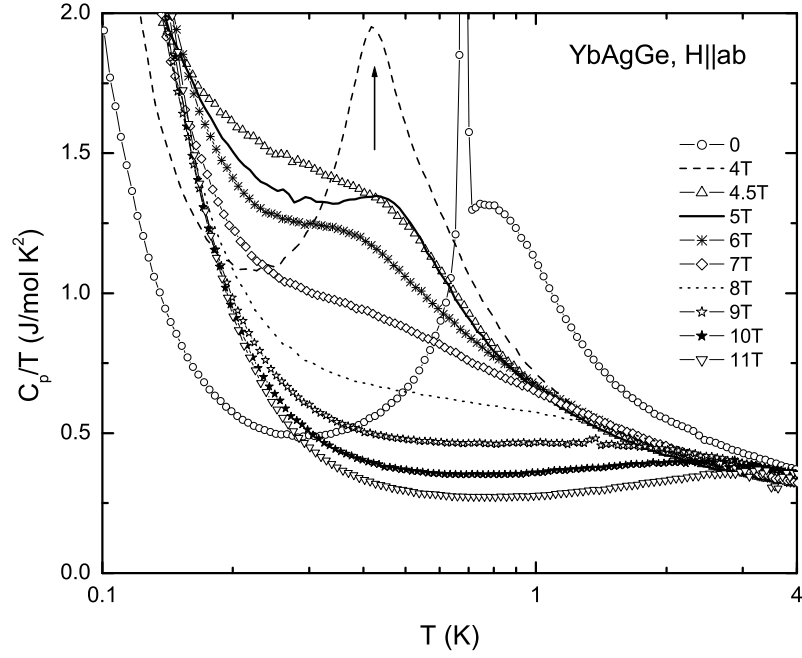


FIG. 5: Low temperature part of the temperature-dependent heat capacity of YbAgGe ($H||ab$) plotted as C_p/T vs. T on a semi-log plot. Arrow marks magnetic transition in $H = 4$ T curve.

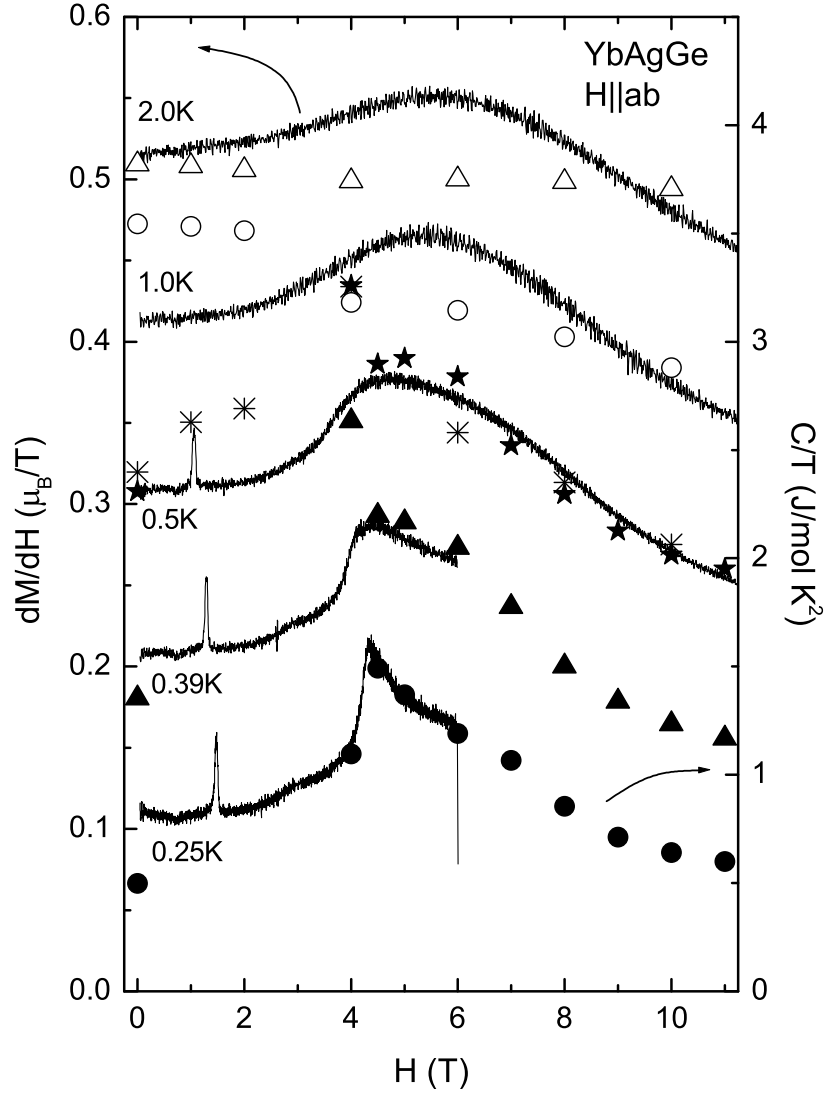


FIG. 6: Low temperature differential susceptibility, dM/dH , and Sommerfeld coefficient, C/T , as a function of applied magnetic field. Data for $T \geq 0.39$ K are shifted vertically by multiplicative of $0.1 \mu_B/T$ (dM/dH) and multiplicative of 0.825 J/mol K^2 (C/T) respectively for clarity. Asterisks and open symbols - C/T obtained using the data from Ref. 1, other symbols - this work.

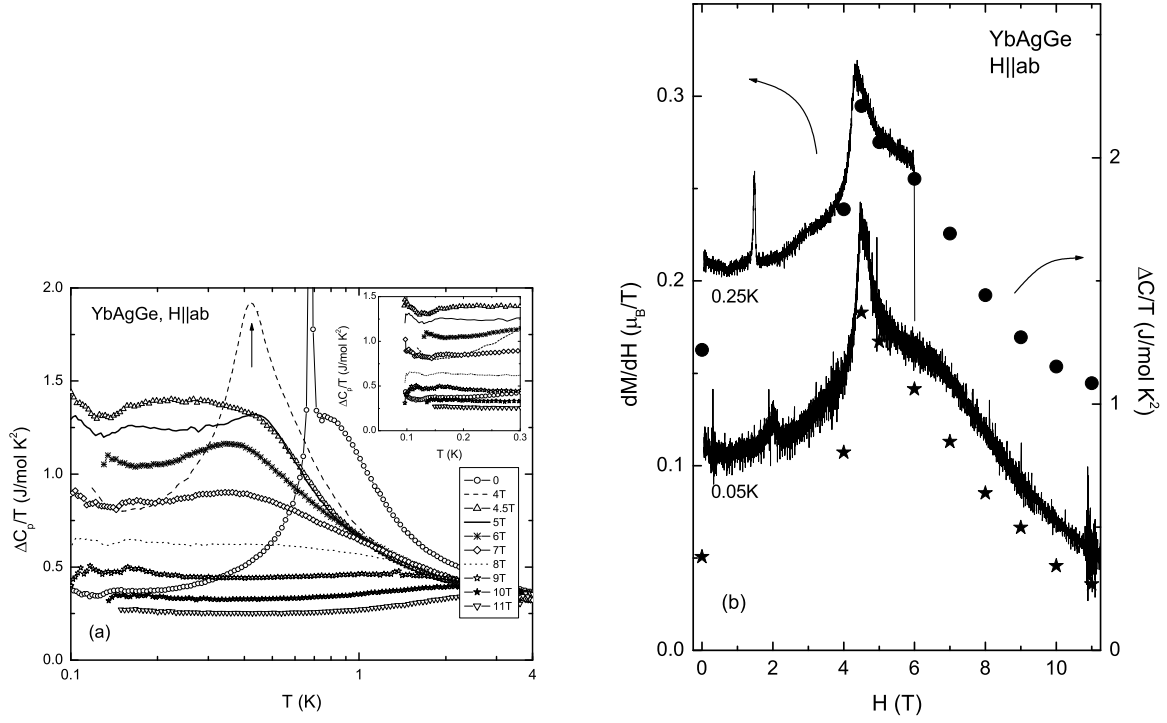


FIG. 7: (a) Low temperature part of the temperature-dependent heat capacity of YbAgGe ($H||ab$), with nuclear contributions subtracted, plotted as $\Delta C_p/T$ vs. T on a semi-log plot. Arrow marks magnetic transition in $H = 4$ T curve; (b) Low temperature differential susceptibility, dM/dH , and Sommerfeld coefficient, C/T , with nuclear contributions subtracted, as a function of applied magnetic field. Data for $T = 0.25$ K are shifted vertically by $0.1 \mu_B/T$ (dM/dH) and 0.825 J/mol K² (C/T) for clarity.

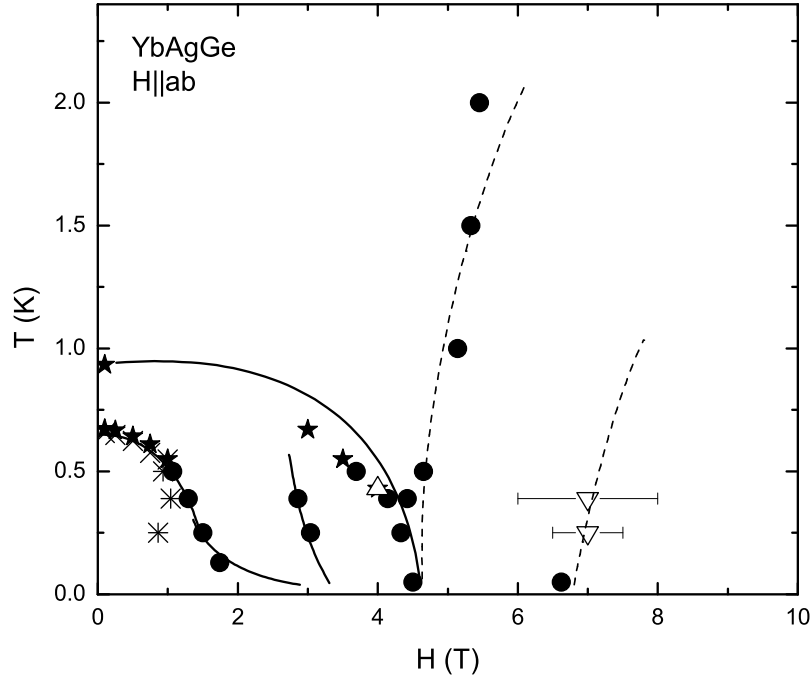


FIG. 8: $H - T$ phase diagram of YbAgGe ($H \parallel ab$): solid lines: magnetic phase lines [1, 7], dashed lines - Hall effect lines [6, 8], symbols - data from this work: \bullet - from field-up $M(H)$ data, \star - from $M(T)$ data taken on increase of temperature, $*$ - from field-down $M(H)$ data, \times - from $M(T)$ data taken on temperature decrease, and \triangle , ∇ - from heat capacity data plotted as $C_p(T)$ and $C(H)/T$ respectively.